九州医療科学大学
がん細胞研究所　研究誌

Journal of Cancer Cell Research Institute
Volume 2　　March, 2026

がん細胞研究所
Cancer Cell Research Institute
あなたの学びを　あなたのカタチに
九州医療科学大学
Kyushu University of Medical Science

目次

研究組織

研究員（学内）

教授 (所長)	三苫 純也	九州医療科学大学 生命医科学部 生命医科学科
教授	池脇 信直	九州医療科学大学 生命医科学部 生命医科学科
教授	坂本 博	九州医療科学大学 生命医科学部 生命医科学科
教授	竹ノ内 博之	九州医療科学大学 生命医科学部 生命医科学科
教授	野村 創	九州医療科学大学 生命医科学部 生命医科学科
教授	宮本 朋幸	九州医療科学大学 生命医科学部 生命医科学科
教授	薬師寺 宏匡	九州医療科学大学 生命医科学部 生命医科学科
教授	山本 成郎	九州医療科学大学 生命医科学部 生命医科学科
特別教授 (専任)	西村 篤乃	九州医療科学大学 生命医科学部 生命医科学科
准教授	西森 誠	九州医療科学大学 生命医科学部 生命医科学科
講師	芝原 一樹	九州医療科学大学 生命医科学部 生命医科学科
講師	二反田 隆夫	九州医療科学大学 生命医科学部 生命医科学科

研究員（学外）

病理診断部長	林 透	潤和会記念病院

Association Between Cell Size and Cancer Stem Cell–Related Properties in Breast Cancer Cell Lines

Tomoyuki Miyamoto, Taiki Yahara.

Cancer cell institute, Kyushu Univ. of Medical Sciences.

Abstract

Background:
Cancer stem cells (CSCs) are implicated in tumor initiation, progression, and recurrence. While CSCs are commonly identified using cell surface markers, their morphological characteristics remain insufficiently characterized. This study investigated whether cell size is associated with CSC-related properties in breast cancer cell lines.

Methods:
Human breast cancer cell lines MDA-MB-231, MCF-7, and SK-BR-3 were fractionated into small (S), medium (M), and large (L) populations based on forward scatter intensity by fluorescence-activated cell sorting. Morphological features were evaluated using cytological staining and image analysis. Tumorigenicity, proliferative capacity, and migratory ability were assessed using soft-agar colony formation assays, CCK-8 assays, and wound healing assays, respectively. Expression of hormone receptors, proliferation markers, epithelial–mesenchymal transition (EMT) markers, and stemness-related genes was analyzed by RT-PCR.

Results:
Image analysis demonstrated significant differences in cell and nuclear areas among size-defined populations. Soft-agar assays revealed that tumorigenic potential was enriched in small-to-medium-sized cells in MDA-MB-231 and MCF-7, and in medium-sized cells in SK-BR-3. Small-to-medium-sized cells showed increased migratory activity and enhanced expression of EMT-related genes, including SNAIL. In MCF-7 cells, these populations also exhibited higher expression of estrogen and progesterone receptors and SOX2.

Conclusions:
CSCs are preferentially enriched in small-to-medium-sized breast cancer cells, suggesting that cell size may serve as a simple morphological indicator of CSC-associated properties.

Introduction

Breast cancer is one of the most common malignant tumors worldwide and represents the second leading cause of cancer-related death among women [1]. In recent years, the incidence of breast cancer has also been increasing in Japan, which is attributed to westernization of dietary habits, lack of childbirth or breastfeeding history, and an increase in the age at first childbirth [2].

Based on biological characteristics, breast cancer is broadly classified into three major subtypes: estrogen receptor (estrogen receptor; ER) and progesterone receptor (progesterone receptor; PR)–positive breast cancer, human epidermal growth factor receptor type 2 (HER2)–positive breast cancer, and triple-negative breast cancer (triple negative breast cancer; TNBC), which lacks expression of ER, PR, and HER2. While ER/PR-positive and HER2-positive breast cancers are generally associated with a favorable prognosis, TNBC is characterized by an aggressive clinical course and poor prognosis [3,4].

Hormone therapy is effective for ER/PR-positive breast cancer, and molecular-targeted therapy using trastuzumab (Herceptin) is established for HER2-positive breast cancer. In contrast, there are currently no effective targeted therapies for TNBC, and its poor prognosis highlights the urgent need for the development of novel therapeutic strategies [5].

Accumulating evidence suggests that cancer stem cells (cancer stem cells; CSCs) play a critical role in tumor recurrence and metastasis, which are major determinants of poor prognosis in breast cancer and other malignancies [6]. CSCs constitute a very small subpopulation within tumors but possess high tumorigenic potential and enhanced invasive capacity through epithelial–mesenchymal transition (epithelial–mesenchymal transition; EMT). These properties indicate that CSCs are key contributors to cancer progression, recurrence, and metastasis [7,8].

CSCs are characterized by stem cell–like properties, including self-renewal and differentiation capacity, and are therefore involved in tumor growth and maintenance. Moreover, CSCs exhibit resistance to radiotherapy and chemotherapy, making them attractive candidates as novel therapeutic targets and prognostic indicators [9].

Several methods have been established to enrich and isolate CSCs for research purposes. The most commonly used approach involves fluorescence-activated cell sorting (fluorescence-activated cell sorter; FACS) based on the expression of cell surface markers

such as CD133, CD44, and CD24. Another widely used method employs the DNA-binding dye Hoechst 33342 to identify and isolate side population (SP) cells, which are considered to be enriched for CSCs 10-12). In addition, FACS-independent approaches, including sphere formation assays that exploit anchorage-independent growth and in vivo transplantation assays using mouse models, have also been reported [13].

However, the isolation and analysis of CSCs require expensive equipment such as FACS and are time-consuming, making it difficult to detect CSCs in routine clinical practice and to apply them directly to diagnosis or prognostic evaluation at present.

In this context, we focused on the cellular morphology of CSCs. Although numerous studies have investigated CSCs using cell surface markers as indicators, relatively few have examined their morphological characteristics. If CSCs could be identified based on morphological features, this approach could contribute to improved qualitative accuracy in pathological diagnosis.

Therefore, in this study, we aimed to elucidate the morphological characteristics of breast cancer stem cells by fractionating breast cancer cell lines according to cell size and analyzing the CSC properties of each cell population.

Materials & methods

Cell lines and culture conditions

Human breast cancer cell lines MDA-MB-231 (triple-negative; JCRB1559), MCF-7 [ER/PR-positive; JCRB0134], and SK-BR-3 [HER2-positive; NIHS0735] were used. Cells were cultured in high-glucose Dulbecco's modified Eagle's medium (DMEM) supplemented with 10% fetal bovine serum (FBS), 1% non-essential amino acids, and 1% antibiotic–antimycotic solution at 37 °C in a humidified atmosphere containing 5% CO_2.

Cell sorting by size

Cells were detached using 0.2% trypsin–EDTA, resuspended at 2–3 × 10^6 cells/mL, and stained with propidium iodide (PI) for viability exclusion. After washing, cells were resuspended in DMEM containing 2% FBS and subjected to fluorescence-activated cell sorting (FACSAria™ III; BD Biosciences).

Cell populations were gated based on forward scatter (FSC) signals. The smallest and largest approximately 5% of cells were defined as the small (S) and large (L) fractions, respectively, while the middle approximately 20%

was defined as the medium (M) fraction. Sorted cells were collected by centrifugation and used for subsequent analyses.

Morphological analysis

For cytomorphological evaluation, 7.5×10^4 cells from each size fraction were prepared as cytospin slides and stained using May–Giemsa and Papanicolaou methods following standard protocols. After staining, 50 cells per fraction were randomly selected and imaged at ×100 magnification using a digital microscope system. Cell area and nuclear area were measured using ImageJ software.

Soft agar colony formation assay

Anchorage-independent growth was assessed using a soft agar colony formation assay. A base layer of 0.7% agar in DMEM was prepared in 6-cm dishes. Cells (5×10^3 cells/mL) from each fraction were suspended in 0.35% agar and layered onto the base agar. Cultures were maintained for 5 weeks at 37 °C with 5% CO_2, and colonies were counted under a light microscope.

Cell proliferation assay

Cell proliferation was evaluated using the Cell Counting Kit-8 (CCK-8) assay. Cells were seeded in 96-well plates at 3×10^3 cells/well and incubated for 24, 48, or 72 h. CCK-8 reagent was added 4 h prior to measurement, and absorbance was measured at 460 nm using a microplate reader.

Cell migration assay

Cell migration was assessed using a wound healing assay. Cells were seeded into culture inserts placed in 35-mm dishes and allowed to reach confluence. After removal of the inserts, cells were incubated, and wound closure was monitored at 24-h intervals using phase-contrast microscopy. Migration areas were quantified using ImageJ.

RNA extraction and RT-PCR

Total RNA was extracted from 1×10^5 cells per fraction using RNAzol® RT according to the manufacturer's instructions. Complementary DNA (cDNA) was synthesized using oligo(dT) primers and reverse transcriptase. RT-PCR was performed using a standard PCR master mix under the following conditions: initial denaturation at 96 °C for 3 min, followed by 35 cycles of 96 °C for 15 s, 60 °C for 15 s, and 72 °C for 3 min. PCR products were analyzed by electrophoresis on 2% agarose gels. Primer sequences are listed in Table 1.

Statistical analysis

Statistical differences among the three size fractions were analyzed using non-repeated measures analysis of variance (ANOVA). A P value < 0.05 was considered statistically significant.

Results

Morphological analysis

To examine whether cancer stem cells (CSCs) could be enriched based on cell size, cells were fractionated into small (S), medium (M), and large (L) populations and subjected to morphological analysis. May–Giemsa staining revealed that size differences among S, M, and L fractions were microscopically distinguishable in MDA-MB-231 cells, whereas discrimination among size fractions was difficult in MCF-7 cells. In SK-BR-3 cells, only the L fraction could be clearly distinguished from the other fractions (Fig. 1). In contrast, size differences were not readily recognizable in Papanicolaou-stained specimens for any of the three cell lines (data not shown). Quantitative image analysis of May–Giemsa– and Papanicolaou-stained images demonstrated progressive increases in cell area and nuclear area from S to L fractions in all three cell lines. The mean cell areas (μm²) were 241 ± 55 (S), 365 ± 88 (M), and 544 ± 80 (L) in MDA-MB-231; 247 ± 50 (S), 263 ± 75 (M), and 394 ± 123 (L) in MCF-7; and 260 ± 60 (S), 305 ± 49 (M), and 472 ± 95 (L) in SK-BR-3 cells. Mean nuclear areas (μm²) were 120 ± 34 (S), 210 ± 54 (M), and 285 ± 53 (L) in MDA-MB-231; 168 ± 33 (S), 183 ± 48 (M), and 218 ± 49 (L) in MCF-7; and 148 ± 32 (S), 169 ± 32 (M), and 236 ± 59 (L) in SK-BR-3 cells. Significant differences in both cell and nuclear areas were observed among all three size fractions in MDA-MB-231 cells, between S–M and S–L fractions in MCF-7 cells, and between S–L and M–L fractions in SK-BR-3 cells (Fig. 2). In contrast, no significant differences were detected among size fractions in Papanicolaou-stained specimens for any cell line. Based on image analysis, a difference in mean cell diameter of approximately ≥11.4 μm was required for reliable microscopic recognition of size differences.

Tumorigenic potential

To determine which size fractions were enriched for CSCs, tumorigenic potential was evaluated using a soft agar colony formation assay. A higher number of colonies indicates greater tumorigenic capacity. After 5 weeks of culture, the numbers of colonies were 68 ± 6 (S), 57 ± 4 (M), and 8 ± 3 (L) in MDA-MB-231; 148 ± 8 (S), 127 ± 3 (M), and 42 ± 6 (L) in MCF-7; and 28 ± 7 (S), 63 ± 4, and 16 ± 4 (L) in SK-BR-3 cells. In MDA-MB-231 and MCF-7 cells, S and M fractions formed significantly more colonies than the L fraction. In contrast, the M fraction of SK-BR-3 cells formed significantly more colonies than both S and L fractions (Fig. 3), indicating that CSCs were enriched

in small-to-medium-sized cells in MDA-MB-231 and MCF-7, and predominantly in medium-sized cells in SK-BR-3.

Cell proliferation

Because CSC-enriched fractions were mainly observed in small-to-medium-sized cells, cell proliferation was subsequently examined using the CCK-8 assay. At 24 h, absorbance values for MDA-MB-231 cells were 0.453 ± 0.004 (S), 0.474 ± 0.018 (M), and 0.569 ± 0.037 (L), and at 72 h were 1.316 ± 0.026 (S), 1.404 ± 0.018 (M), and 1.578 ± 0.122 (L). For MCF-7 cells, absorbance values at 24 h were 0.393 ± 0.018 (S), 0.391 ± 0.006 (M), and 0.347 ± 0.006 (L), and at 72 h were 0.938 ± 0.046 (S), 0.999 ± 0.049 (M), and 0.748 ± 0.053 (L). For SK-BR-3 cells, absorbance values at 24 h were 0.381 ± 0.022 (S), 0.459 ± 0.025 (M), and 0.415 ± 0.032 (L), and at 72 h were 0.785 ± 0.051 (S), 0.997 ± 0.026 (M), and 0.708 ± 0.032 (L). Large cells exhibited significantly higher proliferative activity in MDA-MB-231, whereas small-to-medium-sized cells showed higher proliferation in MCF-7 and SK-BR-3 cells (Fig. 4).

Cell migration

Cell migration was assessed by wound healing assays, as CSCs are reported to exhibit enhanced migratory capacity. Wound closure was quantified at 24-h intervals. In MDA-MB-231 cells, wound closure at 24 h was 55.3 ± 0.074% (S), 80.0 ± 0.004% (M), and 68.3 ± 0.053% (L), and complete closure was observed in all fractions by 48 h. In MCF-7 cells, wound closure at 24 h was 16.5 ± 0.040% (S), 17.8 ± 0.032% (M), and 11.5 ± 0.017% (L); at 48 h, 59.8 ± 0.126% (S), 60.5 ± 0.028% (M), and 36.3 ± 0.058% (L); at 72 h, 97.7 ± 0.033% (S), 95.4 ± 0.043% (M), and 73.3 ± 0.077% (L). Complete closure was achieved at 96 h in S and M fractions. In SK-BR-3 cells, wound closure remained incomplete even after 72 h, with no marked differences among size fractions. Medium-sized cells exhibited significantly higher migratory activity in MDA-MB-231, whereas small-to-medium-sized cells showed higher migration in MCF-7 cells. No significant differences in migration were observed among size fractions in SK-BR-3 cells (Fig. 5).

mRNA expression analysis

To evaluate differences in gene expression among size fractions, RT-PCR was performed for hormone receptors, proliferation markers, epithelial–mesenchymal transition (EMT) markers, and stemness-related factors. ER and PR expression was not detected in any size fraction of MDA-MB-231 or SK-BR-3 cells. In MCF-7 cells, ER expression was detected in all size

fractions, whereas PR expression was observed in S and M fractions only. Analysis of proliferation-related genes revealed higher expression of Cyclin E1 and Ki-67 in S and M fractions across all three cell lines. EMT marker analysis demonstrated strong expression of E-cadherin and SNAIL in S and M fractions of MDA-MB-231 and MCF-7 cells, while SK-BR-3 cells showed strong SNAIL expression in S and M fractions. N-cadherin expression was not detected in any cell line. Stemness-associated gene expression analysis showed that OCT4, SOX2, and cMYC were not detected in MDA-MB-231 cells. In MCF-7 cells, SOX2 expression was detected in S and M fractions, whereas in SK-BR-3 cells, cMYC expression was detected only in the S fraction (Figs. 6–8).

Discussion

To date, cancer stem cells (CSCs) have been extensively investigated using cell surface markers such as CD133, CD44, and CD24, and breast cancer CSCs are known to exhibit a $CD44^{+}/CD24^{-}$ phenotype [10-12,15]. Although previous studies in squamous cell carcinoma and prostate cancer have suggested that smaller cells possess higher CSC properties, few studies have focused on the relationship between cell morphology and CSC characteristics in breast cancer [16]. Therefore, the present study aimed to clarify the morphological features of breast cancer stem cells by analyzing breast cancer cells fractionated according to cell size.

Flow cytometric analysis of MDA-MB-231, MCF-7, and SK-BR-3 cell lines revealed heterogeneous cell populations with distinct size distributions, which could be separated into small (S), medium (M), and large (L) fractions. Morphological evaluation using May – Giemsa–stained preparations demonstrated that size-based discrimination was visually feasible in MDA-MB-231 cells, whereas it was difficult in MCF-7 and partially in SK-BR-3 cells. However, image-based quantitative analysis revealed statistically significant differences among the size fractions in all cell lines. These findings suggest that a certain minimum difference in cell diameter is required for reliable visual discrimination under microscopy. In contrast, Papanicolaou-stained preparations failed to show clear size differences, likely due to differences in fixation methods [17,18]. Given that May–Giemsa staining preserves a flattened, two-dimensional cellular morphology, it may be more suitable for morphological identification of CSC-enriched populations in cytological specimens.

Tumorigenic potential, a key biological characteristic of CSCs, was evaluated using a soft agar colony formation assay. In MDA-MB-231 and MCF-7 cells, S and M fractions exhibited significantly higher colony-forming ability than L fractions, whereas in SK-BR-3 cells, the M fraction showed the highest tumorigenic potential. These results indicate that CSCs are preferentially enriched in small-to-medium-sized cells. This observation is consistent with previous reports demonstrating that smaller cells exhibit enhanced tumorigenicity in other cancer types and in undifferentiated cell populations, including induced pluripotent stem cells [16,19]. In contrast, studies of normal mammary glands have reported higher stemness in larger cells, suggesting that morphological characteristics of CSCs may differ from those of normal tissue stem cells 20).

Analyses of cell proliferation and migration revealed cell line–dependent patterns. In MDA-MB-231 cells, S and M fractions—enriched in CSCs—exhibited low proliferative activity but high migratory capacity, consistent with previously reported CSC characteristics [14]. In contrast, S and M fractions of MCF-7 and SK-BR-3 cells showed relatively higher proliferative activity, suggesting the presence of actively cycling CSCs 21). Poor adhesion and reduced proliferation observed in L fractions, particularly in MCF-7 and SK-BR-3 cells, may reflect cellular swelling associated with cell death, such as necrosis [22].

Gene expression analysis revealed size-dependent differences in hormone receptor expression. In MCF-7 cells, ER expression was detected in all size fractions, while PR expression was preferentially observed in S and M fractions, indicating enhanced hormone dependency in smaller cells. Given that CSCs were enriched in these fractions, CSCs in ER/PR-positive breast cancer may exhibit increased hormone responsiveness, which could contribute to endocrine therapy resistance.

Regarding cell cycle–related genes, Cyclin E1 expression was predominantly observed in S and M fractions across all cell lines, suggesting enhanced proliferative signaling in smaller cells. However, discrepancies between Cyclin E1 expression and proliferation assays, particularly in MDA-MB-231 cells, indicate that additional cyclins and regulatory pathways may contribute to cell cycle progression.

EMT-related gene expression analysis demonstrated SNAIL expression predominantly in S and M fractions,

suggesting enhanced invasive potential in smaller cells. These findings were largely consistent with migration assay results and support previous reports linking CSCs with EMT activation [8,23-25]. However, in SK-BR-3 cells, discrepancies between gene expression and functional assays were observed, indicating the need for further investigation.

Analysis of stemness-associated genes revealed SOX2 expression in S and M fractions of MCF-7 cells and cMYC expression in the S fraction of SK-BR-3 cells, suggesting maintenance of stemness in small-to-medium-sized cells. SOX2 expression in MCF-7 cells correlated with increased proliferation and EMT-related gene expression, consistent with previous reports linking SOX2 to tumor aggressiveness and therapy resistance [26,27].

In conclusion, the present study suggests that CSCs are preferentially enriched in small-to-medium-sized breast cancer cells. Morphological evaluation using May–Giemsa staining may facilitate the identification of CSC-enriched populations and contribute to improved diagnostic accuracy in cytopathology. Future studies involving additional cancer types will be essential to determine whether these morphological characteristics represent a common feature of CSCs.

Conclusion

Our results demonstrate that breast cancer stem cell–associated properties are preferentially enriched in small-to-medium-sized cells across multiple breast cancer cell lines. Cell size correlates with tumorigenic potential, migratory activity, and expression of EMT- and stemness-related markers, suggesting that morphological assessment based on cell size may serve as a simple and complementary approach to conventional marker-based CSC analysis.

References

1) Mansoori M, Madjd Z, Janani L, et al. Circulating cancer stem cell markers in breast carcinomas: a systematic review protocol. Syst Rev. 2017; 6 (1): 262.
2) Shiko Y, Harada A, Ohashi Y. Secular trends of breast cancer detection rate in Japan: Age, period, birth cohort, and region effects from 2004 to 2015. Japanese Society of Public Health. 2020; 67(9):593-602.

3) Palomeras S, Martinez SR, Puig T. Targeting Breast Cancer Stem Cells to Overcome Treatment Resistance. Molecules. 2018; 23(9): 2193.
4) Marotti JD, de Abreu FB, Wells WA, et al. Triple-Negative Breast Cancer: Next-Generation Sequencing for Target Identification. Am J Pathol. 2017; 187(10): 2133-2138.
5) Shien T, Iwata H. Adjuvant and neoadjuvant therapy for breast cancer. Japanese Journal of Clinical Oncology. 2020; 50(3): 225–229.
6) Ayob AZ, Ramasamy TS. Cancer stem cells as key drivers of tumour progression. J Biomed Sci. 2018; 25(1): 20.
7) Yu Z, Pestell TG, Lisanti MP, et al. Cancer Stem Cells. Int J Biochem Cell Biol. 2012; 44(12): 2144-51.
8) Mani SA, Guo W, Liao MJ, et al. The epithelial-mesenchymal transition generates cells with properties of stem cells. Cell. 2008; 133(4): 704–715.
9) Shibata M, Hoque MO. Targeting Cancer Stem Cells: A Strategy for Effective Eradication of Cancer. Cancers (Basel). 2019; 11(5): 732.
10) Greve B, Kelsch R, Spaniol K, et al. Flow cytometry in cancer stem cell analysis and separation. Cytometry A. 2012; 81(4): 284-93.
11) Shiozawa Y, Nie B, Pienta KJ, et al. Cancer Stem Cells and their Role in Metastasis. Pharmacol Ther. 2013; 138(2): 285-93.
12) Tomiyasu S, Miyamoto T, Mori M, et al. Isolation of side population cells from endometrial cancer cells using violet laser diode. Hum Cell. 2014; 27(1): 36-42.
13) Lombardo Y, de Giorgio A, Coombes CR, et al. Mammosphere formation assay from human breast cancer tissues and cell lines. J vis Exp. 2015.
14) Lamb R, Lisanti MP, Clarke RB, et al. Co-ordination of cell cycle, migration and stem cell-like activity in breast cancer. Oncotarget. 2014; 5(17): 7833-7842.
15) Liu S, Cong Y, Wang D, et al. Breast Cancer Stem Cells Transition between Epithelial and Mesenchymal States Reflective of their Normal Counterparts. Stem Cell Reports. 2014; 2(1): 78–91.
16) Li Q, Rycaj K, Chen X, et al. Cancer stem cells and cell size: A causal link? Semin Cancer Biol. 2015; 35: 191–199.
17) Yang GC. The mathematical basis for the increased sensitivity in cancer detection in air-dried cytopreparations. Mod Pathol. 1994; 7(6): 681-4.
18) Schulte E, Wittekind C. The influence of the wet-fixed Papanicolaou and the air-dried Giemsa techniques on nuclear

parameters in breast cancer cytology: a cytomorphometric study. Diagn Cytopathol. 1987; 3(3): 256-61.
19) Osawa Y, Miyamoto T, Ohno S, et al. Morphological Analysis of Live Undifferentiated Cells Derived from Induced Pluripotent Stem Cells. Stem Cells Dev. 2018; 27(1): 1-9.
20) Machado HL, Kittrell FS, Edwards D, et al. Separation by Cell Size Enriches for Mammary Stem Cell Repopulation Activity. Stem Cells Transl Med. 2013; 2(3): 199–203.
21) Huang R, Rofstad EK. Cancer stem cells (CSCs), cervical CSCs and targeted therapies. Oncotarget. 2017; 8(21): 35351–35367.
22) Nikoletopoulou V, Markaki M, Palikaras K, et al. Crosstalk between apoptosis, necrosis and autophagy. Biochimica et Biophysica Acta. 2013; 1833(12): 3448-3459.
23) Rakha EA, Rehim DAE, Pinder SE, et al. E-cadherin expression in invasive non-lobular carcinoma of the breast and its prognostic significance. Histopathology. 2005; 46: 685–93.
24) Mrozik KM, Blaschuk OW, Cheong CM, et al. N-cadherin in cancer metastasis, its emerging role in haematological malignancies and potential as a therapeutic target in cancer. BMC Cancer. 2018; 18: 939.
25) Wang Y, Shi J, Chai K, et al. The Role of Snail in EMT and Tumorigenesis. Curr Cancer Drug Targets. 2013; 13(9): 963–972.
26) Novak D, Huser L, Elton JJ, et al. SOX2 in development and cancer biology. Seminars in Cancer Biology. 2020; 67(1): 74-82.
27) Herreros VM, Zhang JS, Koenig A, et al. SOX2 promotes dedifferentiation and imparts stem cell-like features to pancreatic cancer cells. Oncogenesis. 2013; 2: 61.

Table 1. Primer sequences used for RT-PCR analysis.

Gene	Forward primer (5′ →3′)	Reverse primer (5′ →3′)
GAPDH	AGTCAACGGATTTGGTCG	GGGATTTCCATTGATGACAAGC
ER	GGCATTCTACAGGCCAAATTCAG	CATTTTCCCTGGTTCCTGTCCAAGAGC
PR	CAACTACCTGAGGCCGGATTCAGA	GTTGTTGACAAGATCATGCAAGTTATC
Cyclin E1	CTGCCTGTACTGAGCTGGGCAAATAGAG	GCTCGGGCTTTGTCCAGCAAATCCA
p27	GATGTCAAACGTCGAGTGTCTAACGGG	CATATCTTAATTCGAGCTGTTTACGT
Ki-67	GAAAATCATCAAGGAACAGCCTCAACC	GAACACATTTCCTCCAAAACCTCTG
E-cad	GAAAACAGCAAGGGCTTGGA	TTAGGGCTGTGTACGTGCTG
N-cad	ATCGAAGGATGTGCATGAAGG	TGGCCACTGTGCTTACTGAA
SNAIL	TAGCGAGTGGTGTTCTCTGCG	CATTCGGGAGAAGGTCCGAG
OCT4	AGAGAGGGGTTGAGTAGTCCCTTCGCA	CAAGAGCATCATTGAACTTCACCTTC
SOX2	CACAGCGCCCGCATGTACAACATGATGG	GAGTGGGAGGAAGAGGTAACCACAGG
cMYC	GTGGAAAACCAGCAGCCTCCCGCGAC	GTTCTCCTCAGAGTCGCTGCTGGTG

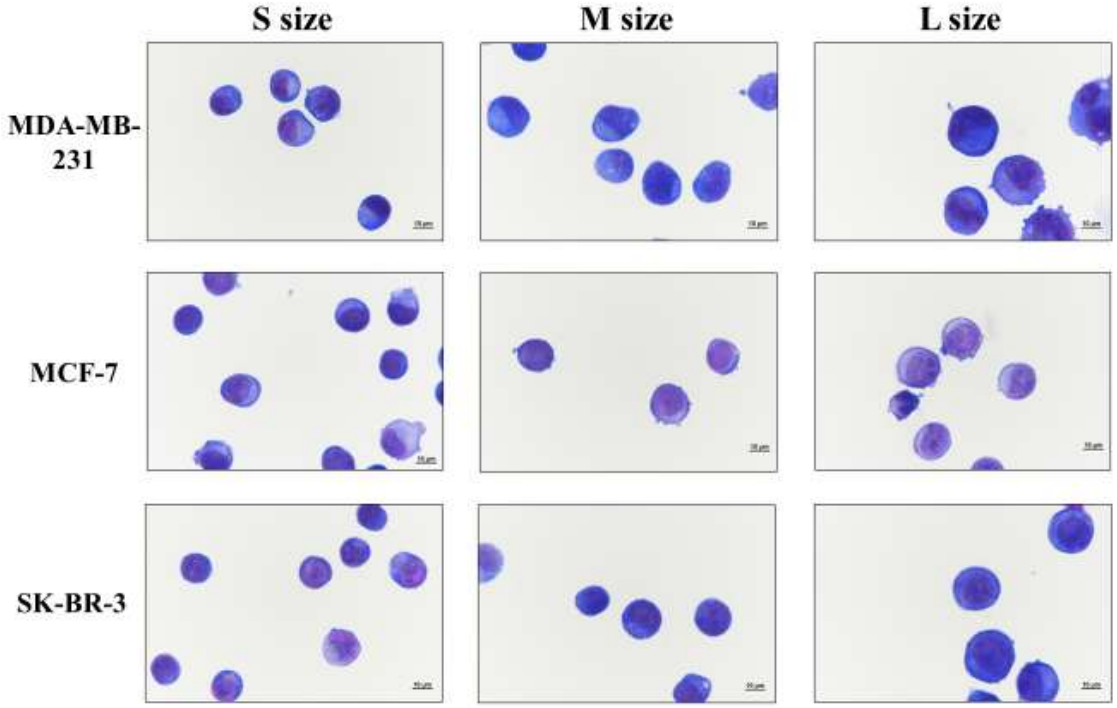

Figure 1. May–Giemsa–stained images of size-fractionated breast cancer cells (objective magnification ×100).

To assess whether size differences among sorted cells could be visually recognized under light microscopy, size-fractionated cells were stained with May–Giemsa and compared. In MDA-MB-231 cells, differences among small (S), medium (M), and large (L) fractions were readily distinguishable. In contrast, size-based discrimination was difficult in MCF-7 cells. In SK-BR-3 cells, size differences were visually apparent only in the L fraction. A total of 50 cells were evaluated per fraction (n = 50).

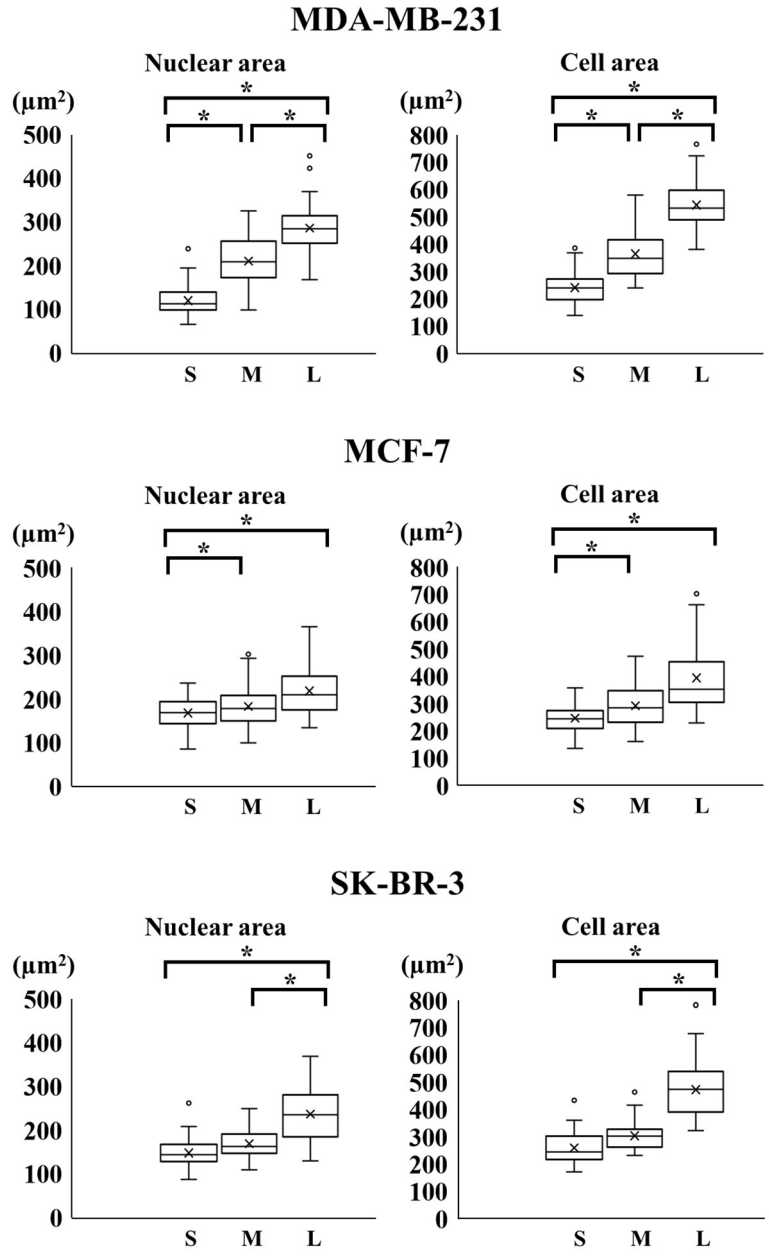

Figure 2. Statistical analysis of nuclear area and cell area based on image analysis. Image-based quantitative analysis revealed significant differences in both cell area and nuclear area among the size-fractionated cells, including differences that were not readily discernible by visual inspection under light microscopy. Nuclear area showed a pattern similar to that of cell area. $P < 0.01$ (non-repeated measures ANOVA, $n = 50$).

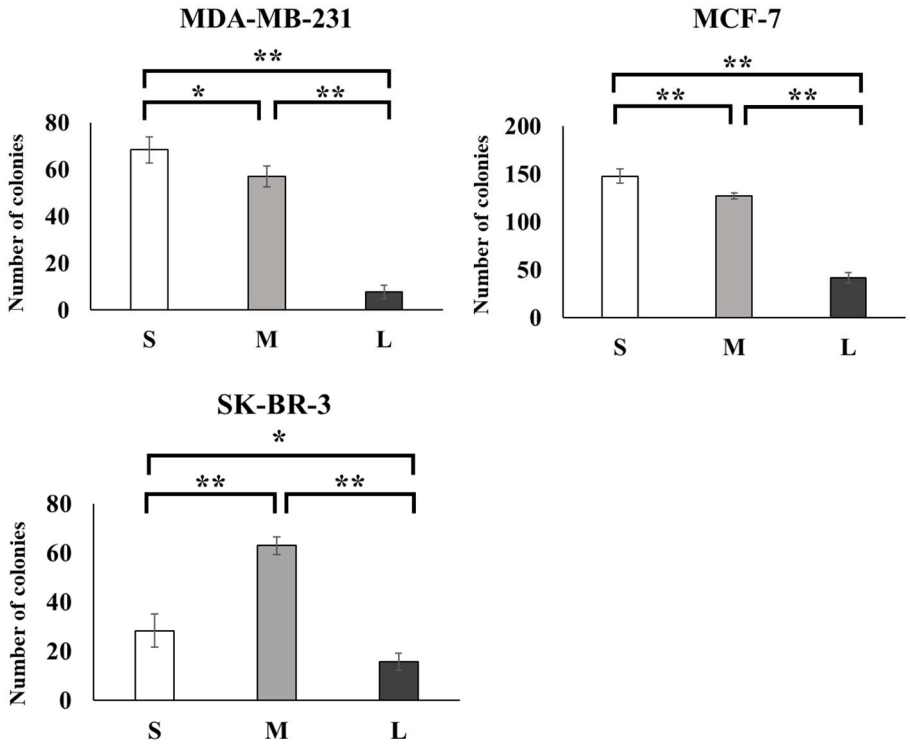

Figure 3. Tumorigenic potential of size-fractionated breast cancer cells.
Tumorigenic potential was evaluated using a soft-agar colony formation assay. In MDA-MB-231 and MCF-7 cells, the small (S) and medium (M) fractions exhibited significantly higher colony-forming ability than the large (L) fraction, whereas in SK-BR-3 cells, the M fraction showed the highest tumorigenic potential. These findings indicate enrichment of cancer stem cell–like properties in the small-to-medium fractions of MDA-MB-231 and MCF-7 cells and in the medium-sized fraction of SK-BR-3 cells. $P < 0.05$, $P < 0.01$ (non-repeated measures ANOVA, $n = 3$).

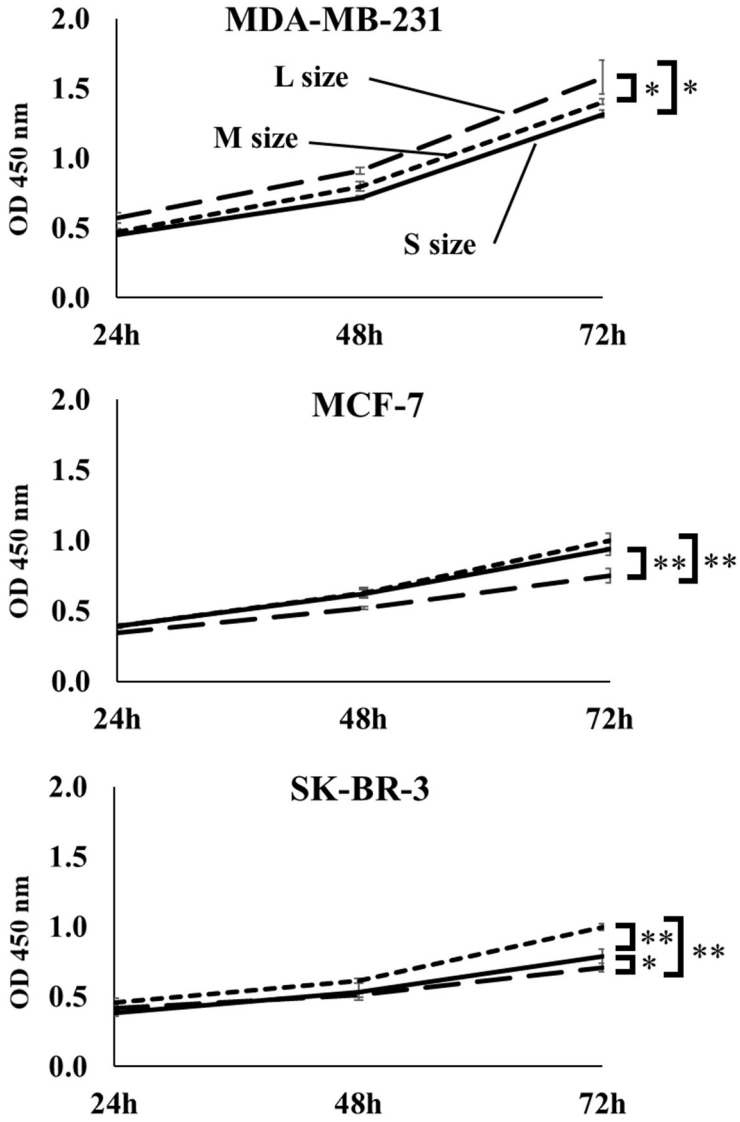

Figure 4. Cell proliferation analysis of size-fractionated breast cancer cells.
Cell proliferation was assessed using the Cell Counting Kit-8 (CCK-8) assay, in which absorbance correlates with cell number. The large (L) fraction of MDA-MB-231 cells exhibited significantly higher proliferative activity, whereas the small (S) and medium (M) fractions of MCF-7 cells and the M fraction of SK-BR-3 cells showed significantly increased proliferation. $P < 0.05$, $P < 0.01$ (non-repeated measures ANOVA, $n = 3$).

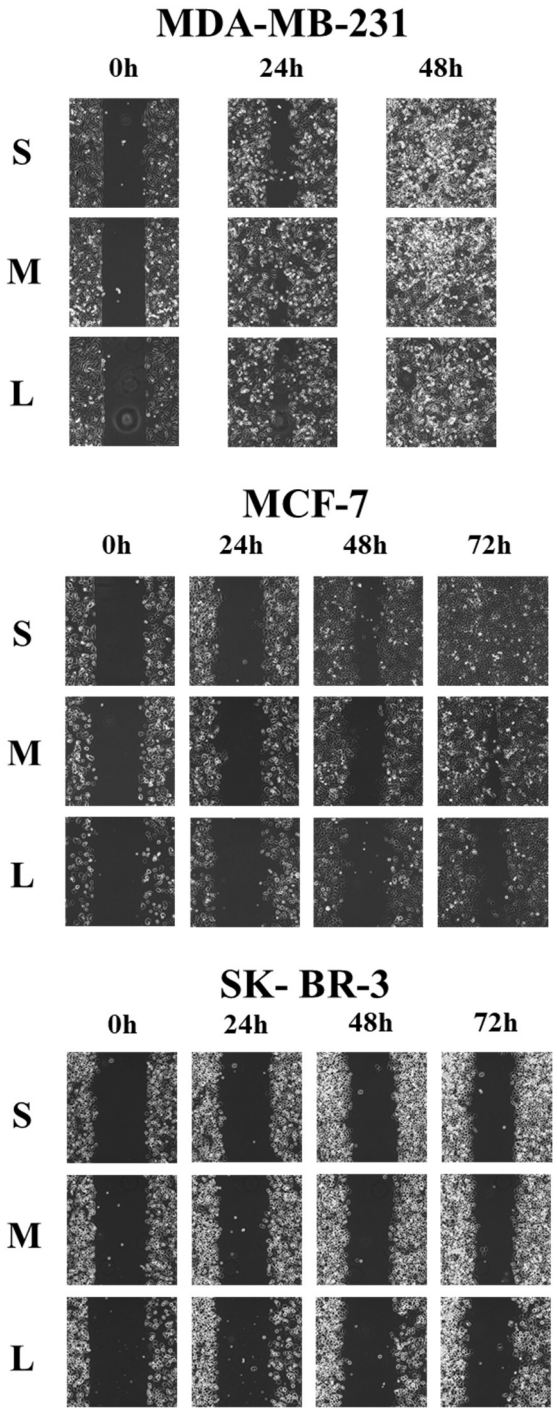

Figure 5. Cell migration analysis of size-fractionated breast cancer cells.
Cell migratory activity was evaluated using a wound healing assay (WHA). Medium-sized (M) MDA-MB-231 cells and small-sized (S) MCF-7 cells exhibited higher migratory capacity, whereas no clear size-dependent differences were observed in SK-BR-3 cells, all of which showed low migratory activity (n = 3).

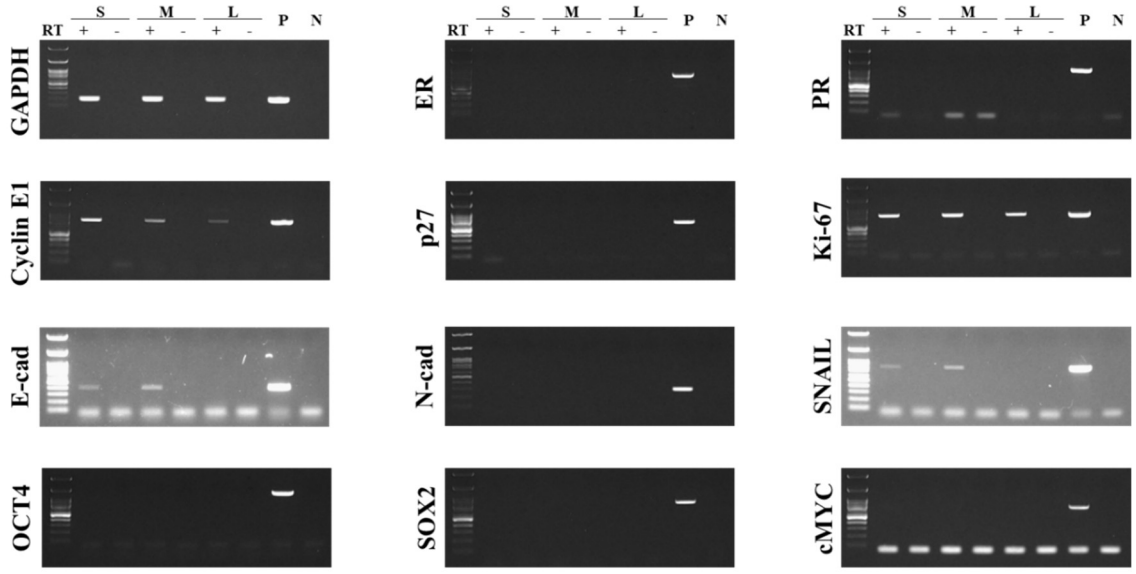

Figure 6. Gene expression analysis of size-fractionated MDA-MB-231 cells.

Gene expression of hormone receptors, cell proliferation markers, epithelial–mesenchymal transition (EMT) markers, and OSKM factors was analyzed by RT-PCR. Expression of Cyclin E1, E-cadherin (E-cad), and SNAIL was detected in the small (S) and medium (M) fractions, suggesting enhanced proliferative and invasive potential in these cells. In contrast, ER, PR, p27, N-cadherin (N-cad), OCT4, SOX2, and cMYC were not detected in any size fraction (n = 3).

P, positive control; N, negative control; RT, reverse transcription.

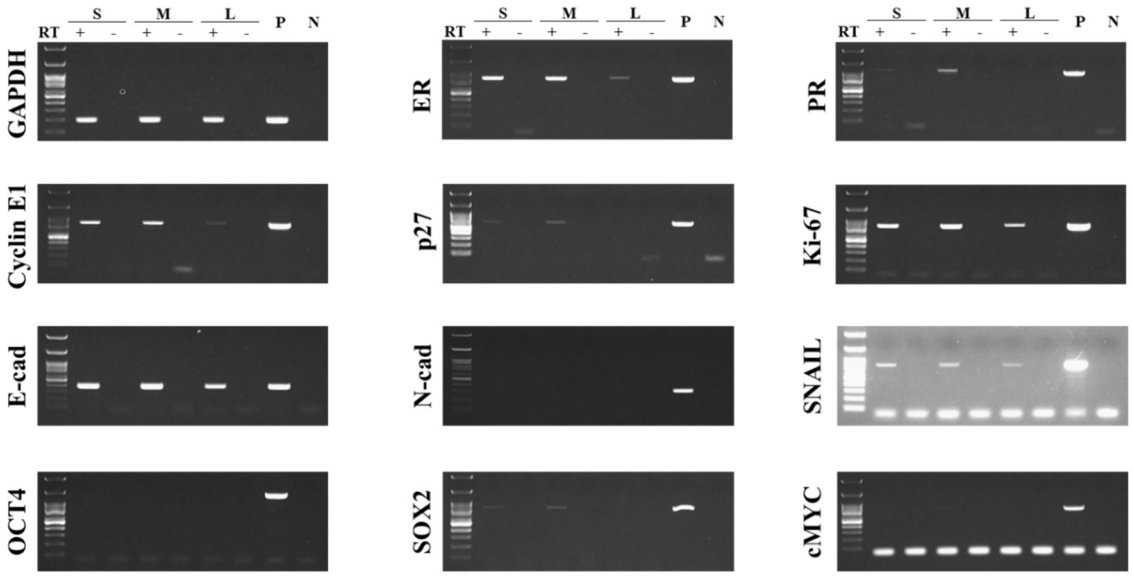

Figure 7. Gene expression analysis of size-fractionated MCF-7 cells.

Gene expression of hormone receptors, cell proliferation markers, epithelial–mesenchymal transition (EMT) markers, and OSKM factors was analyzed by RT-PCR. Stronger expression of ER, PR, Cyclin E1, Ki-67, E-cadherin (E-cad), SNAIL, and SOX2 was observed in the small (S) and medium (M) fractions, while p27 expression was detected predominantly in the M fraction. These findings suggest enhanced hormone dependence, proliferative and invasive potential, and maintenance of stemness in small-to-medium-sized cells. In contrast, N-cadherin (N-cad), OCT4, and cMYC were not detected in any size fraction (n = 3).

P, positive control; N, negative control; RT, reverse transcription.

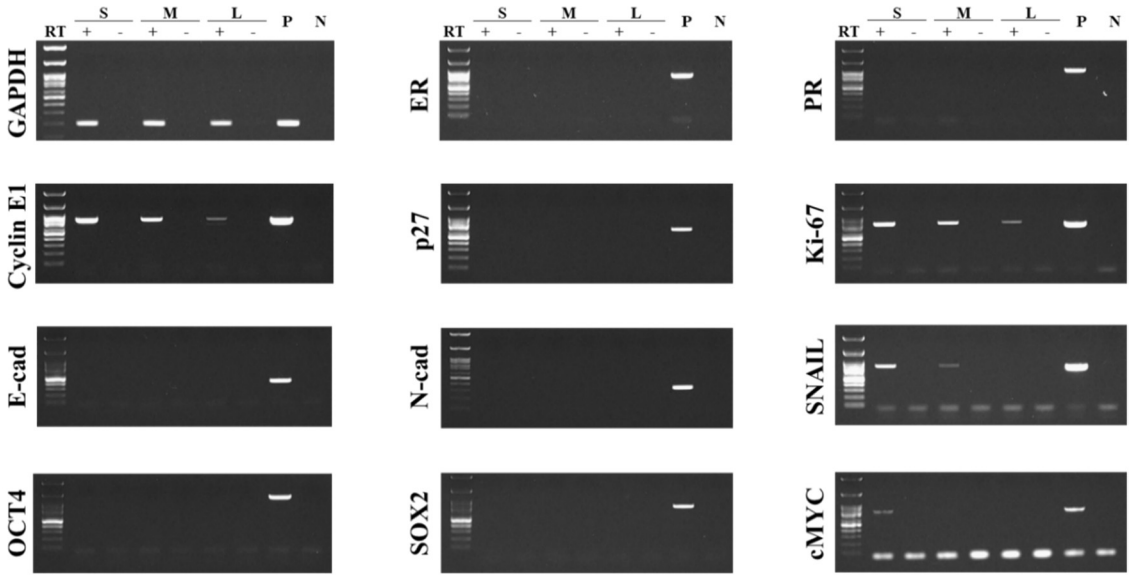

Figure 8. Gene expression analysis of size-fractionated SK-BR-3 cells.
Gene expression of hormone receptors, cell proliferation markers, epithelial–mesenchymal transition (EMT) markers, and OSKM factors was analyzed by RT-PCR. Expression of Cyclin E1, Ki-67, and SNAIL was detected in the small (S) and medium (M) fractions, while cMYC expression was observed exclusively in the S fraction. These results suggest enhanced proliferative and invasive potential in small-to-medium-sized cells and maintenance of stemness in small-sized cells. In contrast, ER, PR, p27, E-cadherin (E-cad), N-cadherin (N-cad), OCT4, and SOX2 were not detected in any size fraction (n = 3).
P, positive control; N, negative control; RT, reverse transcription.

がん特異的に増加するシアリダーゼ Neu3 の細胞内輸送機構の解析

山﨑 春海, 三苫 純也

分泌タンパク質や膜タンパク質の分泌経路は古くから研究されおり、10～20 個の疎水的なアミノ酸残基が並ぶシグナル配列を有するタンパク質は、小胞体～ゴルジ装置を経由し、小胞輸送で細胞膜や細胞外へと分泌されることは周知の事実である（Conventional pathway）。この疎水的なシグナル配列を持たない分泌タンパク質や膜タンパク質も多く存在するが、詳細な輸送経路はわかっていない。

今回着目したシアリダーゼ Neu3 は細胞膜に存在するが、疎水的なシグナル配列を持たないため、非定型的な経路（Unconventional pathway）で輸送されると考えられる[1)]。Neu3 は 4 種類の哺乳類シアリダーゼファミリーの中で唯一各種がんで増加する酵素であるため、新たながんマーカーとしての利用や輸送機構を解析することで新規治療薬の開発に貢献できる可能性がある。

本研究では、Neu3 の細胞内輸送機構を解明するために、まず Neu3 の細胞内局在場所を詳細に観察することを目的とした。また、Neu3 は *S*-アシル化されているとの報告があることから、*S*-アシル化による Neu3 の輸送への影響についても調べた。

Neu3 は細胞膜以外にもエンドソーム[3)4)]や、カベオラ[5)]エクソソーム[6)]にも存在することが報告されているため、いくつかの細胞小器官に対するマーカー抗体を用いて蛍光免疫染色を行い、DsRed を融合したタンパク質 Neu3-DsRed を用いて詳細な局在場所の解析を行った（図 1）。マーカー抗体としては、細胞膜マーカーである Na^+/K^+ ATPase、初期エンドソームマーカーである EEA1、カベオラマーカーである Caveolin-1、エクソソームマーカーである Alix、細胞質マーカーである GAPDH を用いた。

Neu3-DsRed の蛍光は細胞膜に観察され、実際に細胞膜マーカーである Na^+/K^+ ATPase との共局在が認められた。更に一部は初期エンドソームマーカーである EEA1 や細胞膜構造であるカベオラマーカーの Caveolin-1 とも蛍光の重なりが認められた。以上のことから Neu3 は主に細胞膜に存在し、一部は初期エンドソームやカベオラにも局在していると考えられる。

近年発表された、Neu3 のアシル化を報告した研究では Acyl-Biotin Exchange（ABE）法を用いて *S*-アシル化の検出が行われた[4)]。ここではこの研究の再現性をとるために、Neu3-DsRed を発現している CHO 細胞を用いて ABE 法を行った（図 2）。*S*-アシル化されている Caveolin-1 では、NH_2OH 処理後のみアビジンビーズに結合した（+NH_2OH, Bound）。一方で *S*-アシル化されていないネガティブコントロールとして使用した Na^+/K^+ ATPase と c-Src では NH_2OH での処理にかかわらず、アビジンビーズに結合しなかった。以上のことから ABE 法によって *S*-アシル化されているかを解析することが可能であることが確認された。この系を用いて Neu3-DsRed について解析したところ、ネガティブコントロールと同じく NH_2OH 存在下であってもアビジンビーズに結合しなかったため、Neu3-DsRed は *S*-アシル化されていないと考えられる。

Walker と Daniotti はヒト Neu3 の *S*-アシル化を調べるために、*S*-アシル化されている Caveolin-1 をポジティブコントロールとして採用し

たが、*S*-アシル化されていないタンパク質を用いたネガティブコントロールの結果が示されていなかった[4)]。従って彼らの実験系では、本来 *S*-アシル化されていないNeu3がアシル化されているという結論に至った可能性がある。今後は、ヒト Neu3 を用いて彼らの実験を私たちの系で追試すること、ABE 法以外の方法で *S*-アシル化されているかどうかを調べること、またタグをできるだけ小さなものに変更して実験を行うことなどの改善を行い、Neu3 の *S*-アシル化に関する研究を進める必要があると考えられる。

今回の研究では、Neu3-DsRed は *S*-アシル化されていないにも関わらず、少なくともその一部は細胞膜やエンドソームへ移行していた。このことは、Neu3の細胞膜などへの移行に、必ずしも*S*-アシル化は必要ではないことを示唆する。ただ、効率の良い膜移行には *S*-アシル化が有効である可能性は残されている。また、*S*-アシル化によって膜への結合が強固になり、局在場所や酵素活性に影響を与えるかもしれない。

Neu3 は疎水性のアミノ酸残基のクラスターがなく、どのように膜に挿入されているかは現時点では解明されていない。ヒト Neu3 が *S*-アシル化を受けているとすると、その修飾によって integral membrane protein となる可能性はある。高塩濃度処理、アルカリ処理等の処理を *in vitro* で行い、膜にどの程度強固に結合しているのかを調べる必要がある。タンパク質によっては細胞膜と細胞質を行き来するものもあり、それが脂質修飾の on/off によって調整されているようなものもある[7)]。Neu3 もそのような調節を受けており、状況によっては細胞膜に多く存在したり、細胞質に多く存在したりする可能性もある。

Neu3 は唯一様々ながんで発現が上昇するノイラミニダーゼである[2)]。Neu3 は、ガングリオシドという比較的マイナーな糖脂質のシアル酸を切断する酵素であるが、その切断が発端となり、細胞膜上で起こるシグナル伝達が変化し、ドミノ倒しのように発がんに関与しているのかもしれない。Neu3の機能を様々な角度から研究し、具体的にどのように発がんに関与しているかを調べていく必要があると考えられる。

【参考文献】

1. 渡邉さと子 (2016). シアリダーゼ Neu3 は Unconventional Pathway で細胞膜に輸送される. 東北医科薬科大学大学院薬学研究科 生態膜情報学教室 修士論文
2. 宮城妙子 (2008). シアリダーゼによる細胞機能の制御とその異常. 生化学, *80*, 13-23.
3. Cirillo F, Ghiroldi A, Fania C, et al. (2016). NEU3 sialidase protein interactors in the plasma membrane and in the endosomes. J. Biol. Chem., *291*, 100615-10624.
4. Walker M & Daniotti J (2017). Human sialidase Neu3 is *S*-acylated and behaves like an integral membrane protein. Sci. Rep., *7*: 4167, doi:10.1038/s41598-017-04488-w.
5. Wang Y, Yamaguchi K, Wada Tadashi, et al. (2002). A close association of the ganglioside-specific sialidase Neu3 with Caveolin in membrane microdomains. J. Biol. Chem., *277*, 26252-26259.
6. Paolini L, Orizio F, Busatto S, et al. (2017). Exosomes secreted by HeLa cells shuttle on their surface the plasma membrane-associated

sialidase NEU3. Biochemistry, *56*, 6401-6408.
7. Gottlieb C, Zhang S, Linder M (2015). The cysteine-rich domain of the DHHC3 palmitoyltransferase is palmitoylated and contains tightly bound zinc. J. Biol. Chem., *290*, 29259-29269.

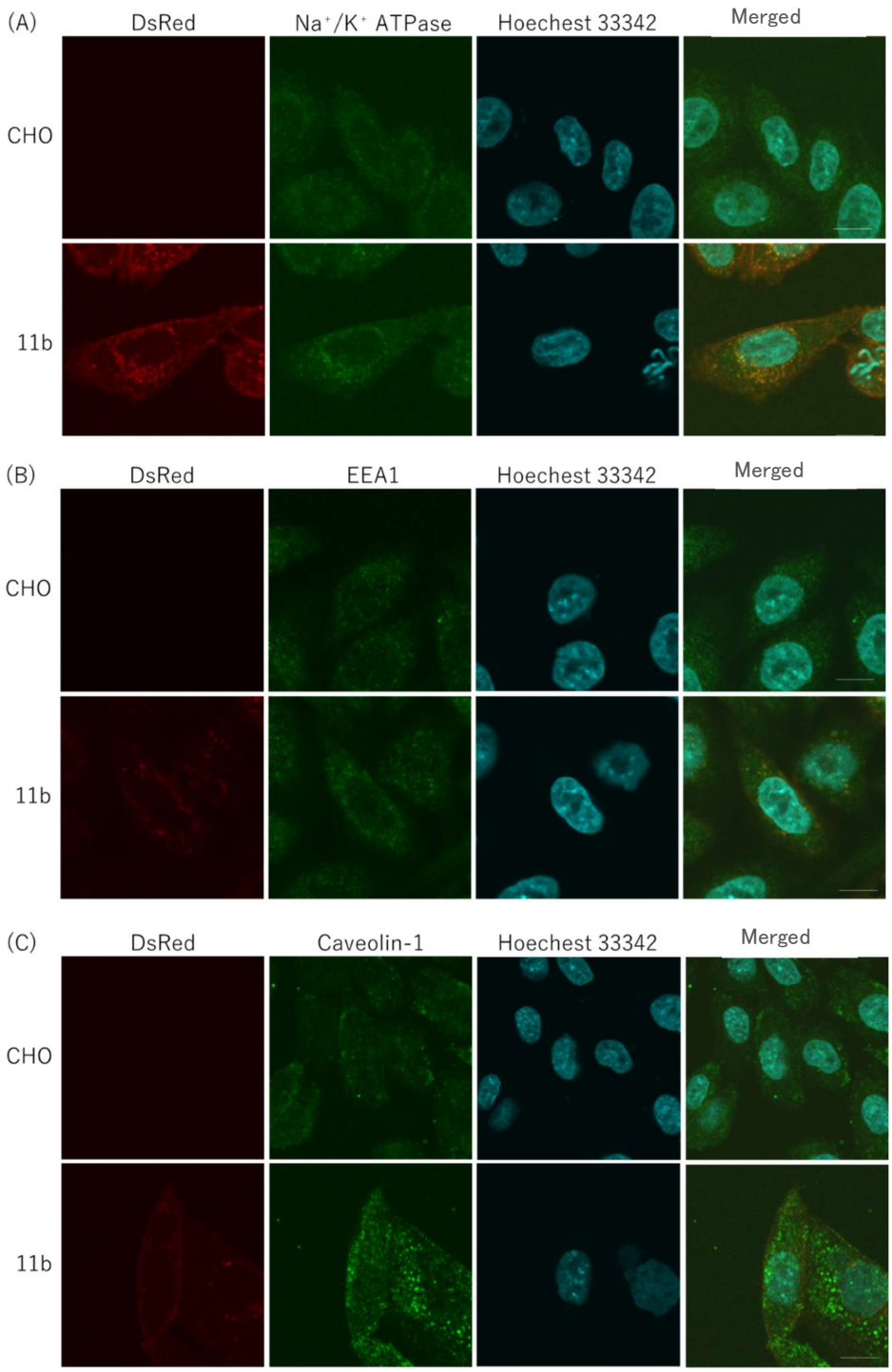
(A)
DsRed
Na⁺/K⁺ ATPase
Hoechest 33342
Merged
CHO
11b
(B)
DsRed
EEA1
Hoechest 33342
Merged
CHO
11b
(C)
DsRed
Caveolin-1
Hoechest 33342
Merged
CHO
11b

図 1. 蛍光免疫染色による Neu3-DsRed の局在解析

（A）細胞膜マーカーである Na^+/K^+ ATPase、（B）初期エンドソームマーカーである EEA1、（C）カベオラのマーカーである Caveolin-1 について、それぞれに対する抗体を用いて蛍光免疫染色を行った。Neu3-DsRed を発現する 11b 細胞では細胞膜および初期エンドソームマーカーである Na^+/K^+ ATPase 及び EEA1 との共局在が認められた。

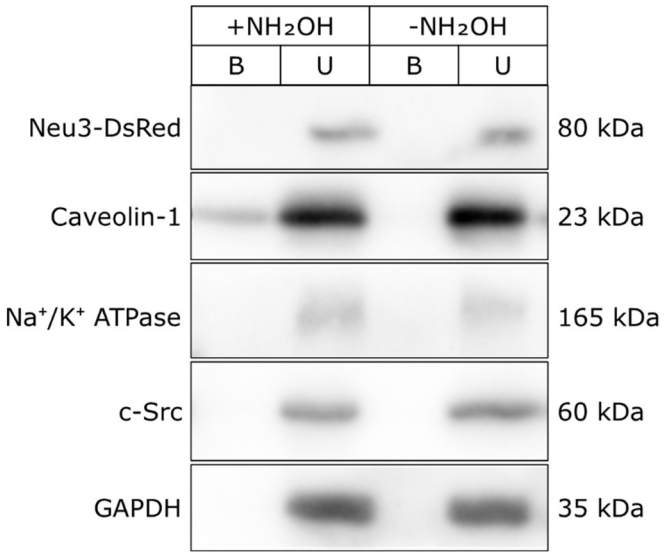

図 2. ABE 法による Neu3-DsRed のアシル化検出

Neu3-DsRed を発現する CHO 細胞を ABE 法で処理し、*S*-アシル化の有無をウエスタンブロット法で解析した。Caveolin-1 はポジティブコントロール、Na^+/K^+ ATPase と c-Src はネガティブコントロールとして使用した。

シアリダーゼ Neu3 の細胞内輸送機構と膜結合性の解析

田中 翼, 三苫 純也

分泌タンパク質や膜で働くタンパク質は、リボソームで翻訳後、細胞内を輸送され、目的場所に到達した後、その機能を発揮する。細胞内輸送経路は 2 種類に大別され、小胞体からゴルジ装置を通り、細胞外や膜へと運ばれる定型経路（Conventional pathway）、小胞体やゴルジ装置を通らずに、細胞外や膜へと運ばれる非定型経路 (Unconventional pathway) が存在する。タンパク質がどちらの経路へ進むかは、そのタンパク質が持つシグナル配列に依存する。大部分の分泌タンパク質や膜で働くタンパク質は、アミノ末端に小胞体移行シグナルといわれるシグナル配列を持つ。そのため、小胞体膜結合型リボソームで翻訳後、小胞体へ移行し、輸送される経路である Conventional pathway を通る。しかし、一部のタンパク質では、小胞体移行シグナル配列がみられず、小胞体を通らずに Unconventional pathway で細胞外や膜まで輸送されるものも存在する。

Unconventional pathway で輸送されると考えられるタンパク質の中に、シアリダーゼ Neu3 という糖加水分解酵素がある [1)]。Neu3 は細胞膜やエンドソームに局在し、糖脂質の一種であるガングリオシド特異的にシアル酸を遊離させる活性を持つ [2)]。この酵素は、現在同定されている 4 種の哺乳類シアリダーゼアイソザイムの中で唯一、大腸癌や腎細胞癌 [3)]、卵巣癌や前立腺癌 [4)]など各種の癌で特異的に増加するアイソザイムであるため、Neu3 の細胞内輸送経路や膜での存在様式を調べることで、これらの癌のメカニズム解明や新たな疾患マーカー、治療標的として有用であると期待される。

現状では、Neu3 は Unconventional pathway で細胞膜へ輸送されると予想されているものの、その詳細な輸送機構や膜への結合様式に関する報告は少ない。そこで本研究ではどのような機構で Neu3 が膜へ輸送され、どのような結合様式をとっているかを調べた。

まず、以下の 4 種のプラスミドすなわち、(1) C 端に Myc-His タグが付加された野生型マウスシアリダーゼ Neu3 (以下、Neu3 とする)、(2) このタンパク質の *N* 末端に小胞体移行シグナルが付加された Neu3 (以下、sig-Neu3 とする)、(3) C 端に Myc-His タグが付加された野生型マウスシアリダーゼ Neu3 に *N* 型糖鎖結合配列が付加された Neu3 (以下、①とする)、(4) これに小胞体移行シグナルを付加した Neu3(以下、sig-①とする)を発現するプラスミドをそれぞれ CHO-K1 細胞に一過性に発現させた。その後、ホモジナイズにより細胞を破壊し、超遠心により膜画分と可溶性画分に分画した。それぞれの画分を電気泳動し、c-Myc を認識する抗体を用いてウエスタンブロッティングを行ったところ (図 1)、小胞体移行シグナル配列で Conventional pathway へ誘導した sig-Neu3 と sig-①、Conventional pathway へ誘導していない Neu3、①は、いずれも膜画分にバンドが見られた。Neu3 と①は 51.5 kDa 付近、sig-Neu3 と sig-①は 53 kDa 付近にバンドが出現すると予想され、確かにその付近にバンドが確認された。sig-①は 4 種類の中で最も上部にバンドが見られたが、これは小胞体で *N* 型糖鎖が付加された

からと考えられる[5)]。

次に、それぞれの Neu3 の膜への結合様式を調べるため、Sodium Carbonate 処理を行った[6)](図 2)。膜タンパク質を 0.1 M Sodium carbonate に暴露すると、膜に強く結合している Peripheral membrane protein は膜から遊離するが、脂質二重層を貫通するように強く結合している Integral membrane protein は遊離せず、超遠心により可溶性画分と膜画分にそれぞれ回収される。4 種類の Neu3 に対して Sodium Carbonate 処理を行った結果、4 種類共に膜画分にバンドが観察された。これらの結果を総合すると、野生型 Neu3 は小胞体を通らずに膜へと輸送され dda、膜に強く結合して Integral membrane protein の様に振る舞っており、小胞体を通る Conventional pathway へ誘導した Neu3 はシグナルペプチドが切断されず、膜に強く結合する Integral membrane protein の様式で存在していると考えられる。

Neu3 には典型的な膜挿入部位である疎水性アミノ酸残基のクラスターがなく、どのようにして膜に強固に結合しているのかは全く分かっておらず、非常に興味深い今後の課題である。

【参考文献】

1. 渡邊さと子. (2016). シアリダーゼ Neu3 は Unconventional pathway で細胞膜に輸送される. 東北医科薬科大学大学院薬学研究科 生体膜情報学教室.
2. 宮城妙子. (2008). シアリダーゼによる細胞機能の制御とその異常. 生化学. 第 80 巻第 1 号, 13-23.
3. S. Ueno, et al. (2006). J. Biol. Chem., *281*, 7756.
4. S. Kawamura, et al. (2012). Plasma membrane-associated sialidase (NEU3) regulates progression of prostate cancer to androgen-independent growth through modulation of androgen receptor signaling. Cell Death Differ., *19*, 170.
5. 立場剣司、前花健太、松崎将士、森悠美. (2018). Unconventional pathway によるシアリダーゼ Neu3 の細胞内輸送の解析. 平成 30 年度卒業論文集 *1*: 1-11.
6. Macarena W, Jose D. (2017). Human sialidase Neu3 is *S*-acylated and behaves an integral membrane protein. Sci. Rep. *7*, 1-13.

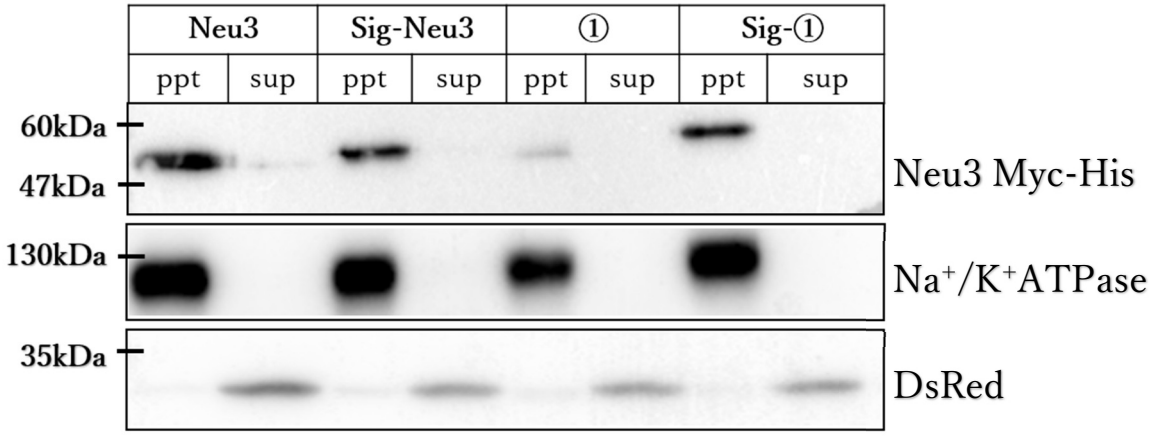

図 1.　4 種類の Neu3 の分布

4 種類の Neu3 誘導体をそれぞれ CHO 細胞に導入し、超遠心により膜画分（ppt）と可溶性画分（sup）に分け、ウエスタンブロット法で細胞内局在を解析した。いずれも ppt にバンドが出現した。

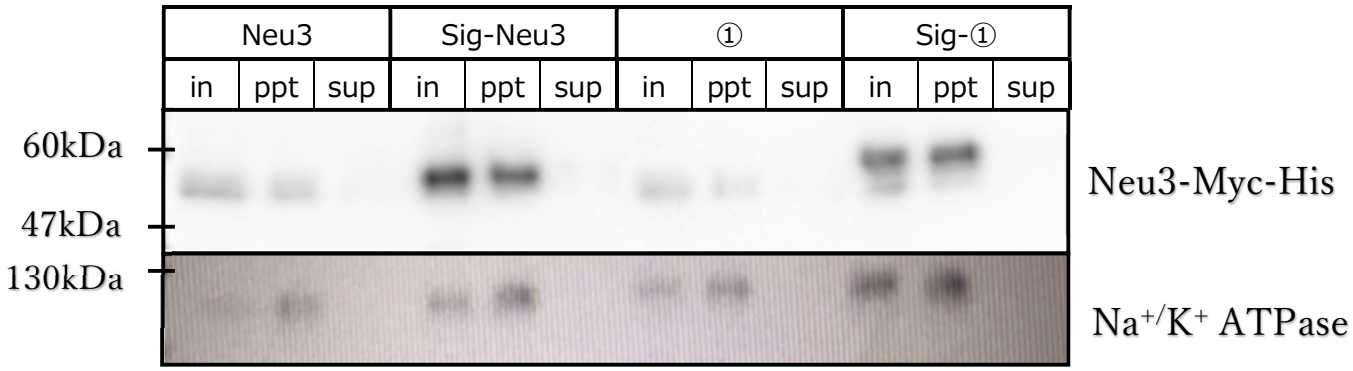

図 2.　4 種類の Neu3 の膜結合性解析

４種類の Neu3 をそれぞれ CHO 細胞に導入し、超遠心により膜画分（ppt）と可溶性画分（sup）に分けた。膜画分を 0.1 M Sodium Carbonate 処理し、ウエスタンブロット法で解析した。いずれも ppt にバンドが出現した。

九州医療科学大学　がん細胞研究所　研究誌
Journal of Cancer Cell Research Institute
Volume 1

発行日　2025 年 3 月 30 日
発行者　学校法人　順正学園
九州医療科学大学　がん細胞研究所
〒882-8508　宮崎県延岡市吉野町　1714-1
TEL 0982-23-5555
編集者　九州医療科学大学　がん細胞研究所　編集委員会